ROLE OF THE SUPPORT ON THE ACTIVITY OF SILICA-SUPPORTED TiO_2 PHOTOCATALYSTS: STRUCTURE OF THE TiO_2/SBA-15 PHOTOCATALYSTS.

María-José López-Muñoz, Rafael van Grieken, José Aguado, Javier Marugán

ESCET. Universidad Rey Juan Carlos. C/ Tulipán s/n, 28933 Móstoles, Madrid, Spain.
Phone: +34 91 664 74 64 ; Fax: +34 91 488 70 68 ; E-mail: mariajose.lopez@urjc.es

Published on:
Catalysis Today, 101: 307-314 (2005)
doi:10.1016/j.cattod.2005.03.017

ABSTRACT

Immobilization of TiO_2 on silica materials has been commonly proposed in order to make easier the separation of the catalyst after the photocatalytic reactions in aqueous systems. The main drawback of the supported photocatalysts is that they usually show lower activities in comparison with powdered TiO_2 materials. The aim of this work is to elucidate the structure of some silica-supported TiO_2 photocatalysts recently developed as well as to evaluate the role that the porous structure of the support can play in the observed photocatalytic activities. In comparison with the use of an amorphous silica support, the use of the mesostructured silica SBA-15 produces an ordered structure in which TiO_2 crystals of similar sizes, independently of titania loading, are located inside the mesoporous channels of the support. The photocatalytic treatment of several cyanide-containing compounds is analyzed and the results are explained in terms of the structure of every catalyst. Depending on the model compound, the characteristic structure of the TiO_2/SBA-15 materials allows increasing up to eight times the photonic efficiency achieved by the Degussa P25 TiO_2. The main conclusion of this work is the strong influence of the textural properties of the support on the catalytic activity of immobilized TiO_2 photocatalysts.

INTRODUCTION

Heterogeneous photocatalysis has shown a high efficiency in the removal of highly toxic and non-biodegradable pollutants commonly present in air and domestic or industrial wastewaters [1-7]. These processes are based on the use of UV radiation to stimulate a semiconductor material, usually TiO_2, on whose surface the oxidation of the pollutant is carried out.

To maximize TiO_2 photoactivity, particles should be small enough to offer a high specific surface area. Unfortunately for applications in aqueous phase such a small particle size means high filtration costs to remove the catalyst once the reaction is finished. These problems have motivated the development of supported photocatalysts in which TiO_2 has been immobilized on diverse materials [8,9].

In addition to some other important properties, it is desirable for a support to be chemically inert, to present a high specific surface area and to be transparent to the UV radiation. Probably this is the reason why most of the work on immobilized photocatalysts has been focused to the use of siliceous materials as supports, for instance: non-porous silica microspheres [10,11], glass [12-15], quartz [13,16] and silica gel [17-25]. An special mention requires the use of silicates or aluminosilicates with zeolitic structures, either crystalline, such as VPI-5 [26] and zeolites X and Y [22,27,28], or mesostructured, such as FSM-16 [29], HMS [22] and MCM-41 [27-29].

Concerning the photocatalyst preparation methods, there are also many procedures reported in the literature. As examples: i) flame oxidation of $TiCl_4$ [10], ii) hydrolysis of $TiCl_3$ [11], iii) chemical vapour deposition [12,24,25], iv) oxidation of metallic titanium [16], v) metal ion implantation [15], vii) immobilization of commercial TiO_2 materials, *e.g.* Degussa P25 [21] and vii) sol-gel [13,14,17-23].

Probably the most widely used materials consist of titanium dioxide synthesized via sol-gel and supported on silica gel. This combination allows a precise control of the properties of the produced materials through the manipulation of the main synthesis variables, in order to maximize the activity of the supported photocatalysts. However, and despite huge efforts, immobilized TiO_2 is commonly reported as less photoactive than the bare TiO_2, with only several exceptions in which the adsorption stage seems to control the global kinetics [30,31].

In a previous work, we reported the synthesis of a new type of supported photocatalysts obtained by controlling the crystal size of TiO_2 through the use of the mesostructured silica SBA-15 as support [32]. These materials presented a lower activity for free cyanide photoxidation than the commercial TiO_2 Degussa P25. However, they showed

unexpected activities for cyanide photoxidation when iron-complexed species were present, leading to much better results than those corresponding to P25 [33]. The aim of the present work is to carry out a detailed characterization of these materials in order to clarify the influence of the structure of the silica support on the photocatalytic activity for several cyanide containing model compounds.

EXPERIMENTAL

Catalysts synthesis and characterization

Two different silica materials were used as supports for the preparation of TiO_2 photocatalysts. The first one was an amorphous SiO_2 commercially available (Grace Sylopol 2104). It presents a wide pore size distribution contrasting with the second silica support, the so-called SBA-15 silica, a mesostructured material with a very well defined pore size in the range of the mesopores (around 6 nm for the material synthesized in this work). The latter was prepared in our laboratory according to the original method of Stucky *et al.* [34].

Incorporation of titania into the supports was carried through a sol-gel method. Hydrolysis of titanium tetraisopropoxide and condensation inside the porous structure of the silica was followed by hydrothermal treatment for the crystallization of TiO_2. A detailed explanation of the synthesis procedure can be found elsewhere [32,33]. Depending of the silica support, the catalysts will be named as x%TiO_2/GrSiO_2 or x%TiO_2/SBA-15 (x represents the wt % of titania loading).

In a previous work, the catalysts were characterized by nitrogen adsorption isotherms at 77 K (Micromeritics Tristar 3000) and powder X-ray diffraction (Philips X'PERT MPD, Cu$K\alpha$ radiation) [32].

In this work, additional characterization has been done in order to clearly establish the structural properties of these materials. Scanning electron microscopy together with energy dispersive X-ray microanalysis was very useful to study the morphology of the particles and the homogeneity in the titania distribution inside the support. SEM micrographs were obtained in a JEOL JSM-6400 working at 20 kV. Transmission electron microscopy was used to evaluate the size distribution of the TiO_2 crystals incorporated into the silica. A JEOL JEM-2000 FX microscope working at 200 kV was used to take the TEM micrographs.

Additionally, a more detailed analysis of the porous structure of the TiO_2/SBA-15 photocatalysts has been done, through argon adsorption-desorption isotherms at 77 K, obtained in a Micromeritics ASAP 2010 sorptometer.

Photocatalytic reactions

The photocatalytic activity of these materials has been tested with different model compounds and their activities have been compared with the results obtained using the commercial TiO_2 sample *Degussa P25*. The experimental setup consists of a batch photoreactor with irradiation by a 150 W medium pressure mercury lamp (Heraeus TQ-150) externally cooled. The catalyst was maintained in suspension by a magnetic stirrer placed at the bottom of the vessel. A gas bubbling system provides the oxygen required for the oxidation reactions or nitrogen in these cases in which reduction is the main process.

The UV-A incident photon flow, determined by ferrioxalate actinometry, was $1.37 \cdot 10^{-5}$ Einstein l^{-1} s^{-1}. All reactions were carried out at room temperature with a catalyst concentration of 0.5 g TiO_2 l^{-1}, having in mind the different titania loading of the catalysts tested. This catalyst concentration has been previously selected from studies with Degussa P25 titania in order to obtain a total absorption of photons. However, the initial cyanide concentration and initial pH value of the solution depends on the model compound.

Potassium cyanide (Panreac, reagent grade) was used for the free cyanide photoxidation runs. The initial conditions for these reactions were a concentration of 3.85 mM KCN and pH value of 11.0. Cyanide decrease was followed by the pyridine-barbituric standard colorimetric method. Oxidation products, mainly cyanate, were analysed by ion chromatography (Metrohm Separation center 733) using an aqueous solution of $NaHCO_3$ (2 mM) and Na_2CO_3 (1.3 mM) as eluent.

Potassium ferricyanide solutions (Panreac, reagent grade) were prepared with an initial concentration of 0.64 mM and pH of 12.0. Total concentration of iron complexed cyanide was determined by ICP/AES (Varian Vista AX), whereas free cyanide and cyanate were analysed by the same methods previously described for potassium cyanide photoxidation runs.

Reactions with potassium dicyanoaurate (Aldrich, 98%) were carried out with an initial concentration of 0.38 mM and pH adjusted to 12.0. Analysis of metal-cyanide complexes was also conducted by ICP/AES and free cyanide and cyanate by the above mentioned methods.

RESULTS AND DISCUSSION

Characterization of the catalysts.

Table 1 summarized the textural properties and average TiO_2 crystal size calculated for these materials, reported in the above commented previous work [32], and required for the discussion. The main conclusion of that work was that the use of the SBA-15 silica support seems to control the TiO_2 crystal size by constraining the growing of the titanium dioxide clusters inside the mesoporous channels. In contrast, the use of an amorphous support does not induce this effect, leading to bigger TiO_2 crystals as the titania loading increases.

Table 1. Textural properties and average TiO_2 crystal size of the supported photocatalyst.

Catalyst	Specific surface area S_{BET} / $m^2\ g^{-1}$	Pore volume V_P / $cm^3\ g^{-1}$	Average pore size D_{BJH} / *nm*	Average TiO_2 crystal size ϕ_{TiO2} / *nm*
Grace SiO_2	317	1.59	19.1	-
20% TiO_2 / $GrSiO_2$	299	1.16	17.1	6.8
40% TiO_2 / $GrSiO_2$	246	0.94	17.5	8.0
60% TiO_2 / $GrSiO_2$	179	0.67	17.3	12.2
SBA-15 SiO_2	640	0.96	6.3	-
20% TiO_2 / SBA-15	532	0.78	6.0	6.2
40% TiO_2 / SBA-15	442	0.69	5.9	6.7
60% TiO_2 / SBA-15	349	0.60	5.8	6.8

In the present work, a more detailed characterization of the supported photocatalysts has been done in order to improve the knowledge of the structure of these materials. From the SEM observations, the TiO_2/$GrSiO_2$ materials consist of 10 – 70 μm particles. Figure 1 (left) shows the SEM micrograph of a fragment of the 20%TiO_2/$GrSiO_2$ catalyst. At the bottom of the photograph the silicon and titanium microanalysis performed by X-ray energy dispersive analysis have been included. As it can be seen, this catalyst shows a granular appearance with a heterogeneous distribution of the silicon and titanium oxides. For instance, titanium dioxide seems to be more concentrated in the upper part of this particle. The analysis of several random particles of this material confirms these results.

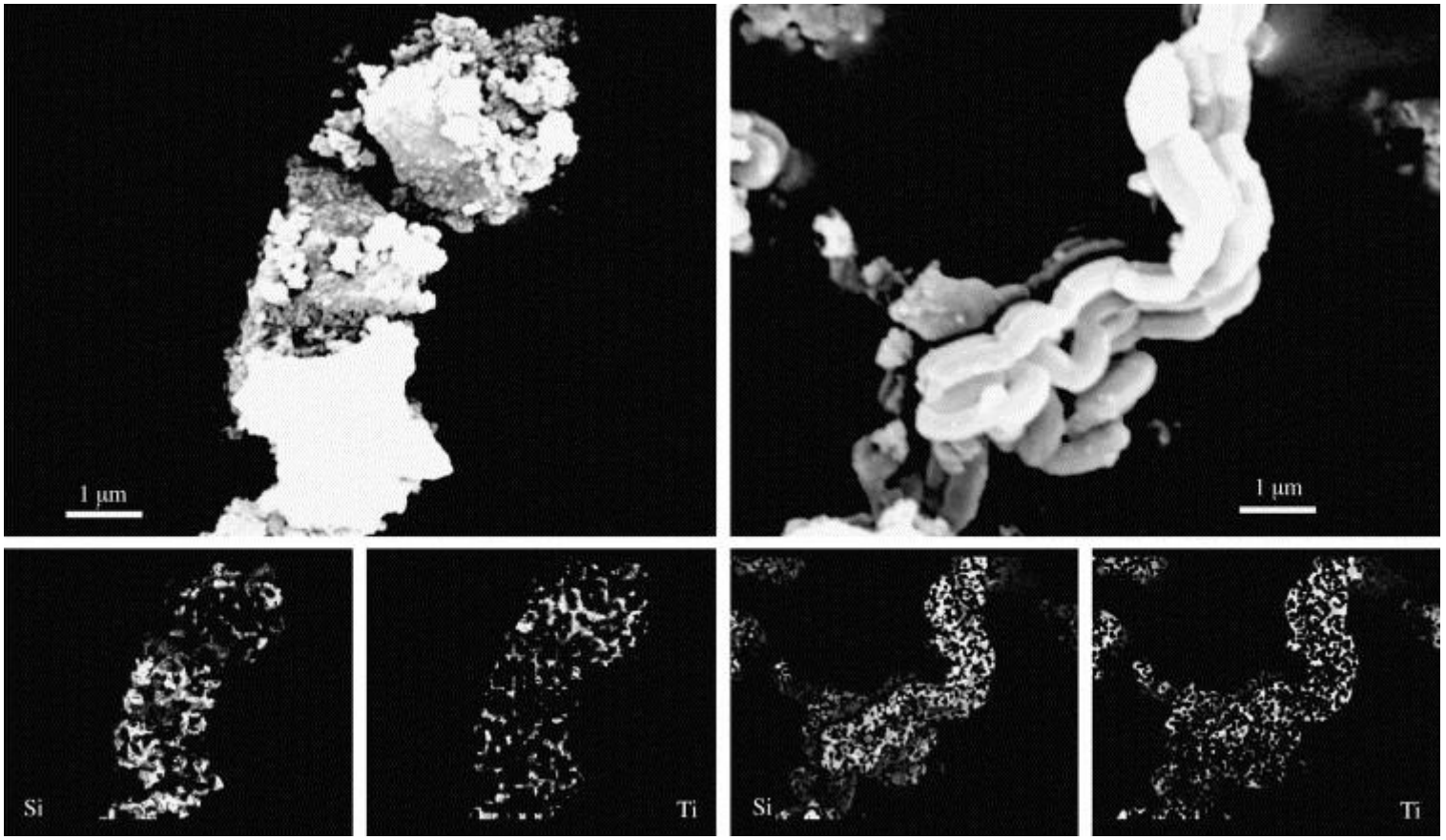

Figure 1. SEM micrographs and EDX maps of silicon and titanium of the catalysts 20%TiO_2/$GrSiO_2$ (left) and 20%TiO_2/SBA-15 (right).

In contrast, as it is shown in the SEM micrograph and EDX maps of figure 1 (right), TiO_2 is apparently more homogeneously distributed in the TiO_2/SBA-15 catalysts. These materials consist of oval shape particles with sizes slightly lower than 1 μm. Maybe this lower size of the silica particles could be responsible of the more homogeneous distribution of the titanium dioxide during the synthesis stage.

In order to find out the crystal size distributions that produce these average values, TEM micrographs were collected. They allow the direct measurement of the size of titanium dioxide particles. However, the small size of the crystals requires such a high enlargement of the image that drastically reduces the number of titania particles observed, making difficult to obtain statistically significant results. Consequently an indirect method was used. A larger area of the catalysts was selected (enough to obtain a substantial amount of TiO_2 crystals) and dark field images were taken. These images are generated by selecting a single direction for electron diffraction. Assuming that the unit cells of the titanium dioxide crystals are randomly orientated, the dark field micrographs produce a statistical high contrast image with very brilliant point whose size depends directly on the crystal size. Figure 2 displays the TEM micrographs and the corresponding dark field images of the same area for the catalysts 20%TiO_2/$GrSiO_2$ and 20%TiO_2/SBA-15.

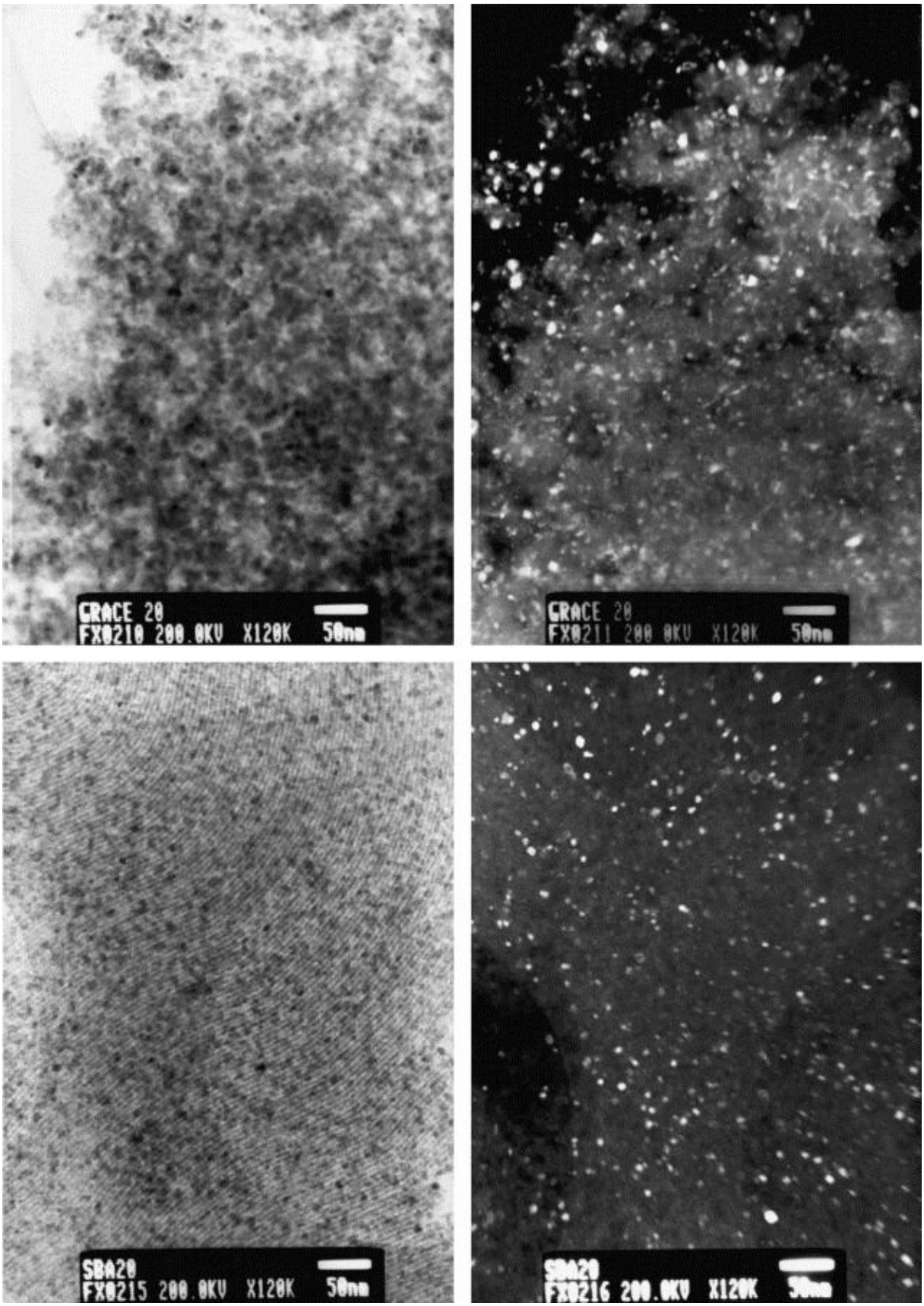

Figure 2. TEM micrographs (left) and dark field images (right) of the catalysts 20%TiO_2/$GrSiO_2$ (top) and 20%TiO_2/SBA-15 (bottom).

At first sight, titanium dioxide crystals of the 20%TiO_2/SBA-15 material seem to have a more uniform size, whereas the $GrSiO_2$ based catalyst presents a wider range of crystal sizes, although to quantify the distribution, a more accurate procedure must be used. High resolution and contrasted micrographs were processing with the software Olympus MicroImage v4.0 using morphological filters of different shapes in order to count automatically the frequency for every crystal size. Calibration was done by selecting several crystals whose size was clearly measured both in the TEM and in the dark field micrographs. Figure 3 represents the crystal size distribution obtained for the catalyst with 20wt% and 60wt% of TiO_2.

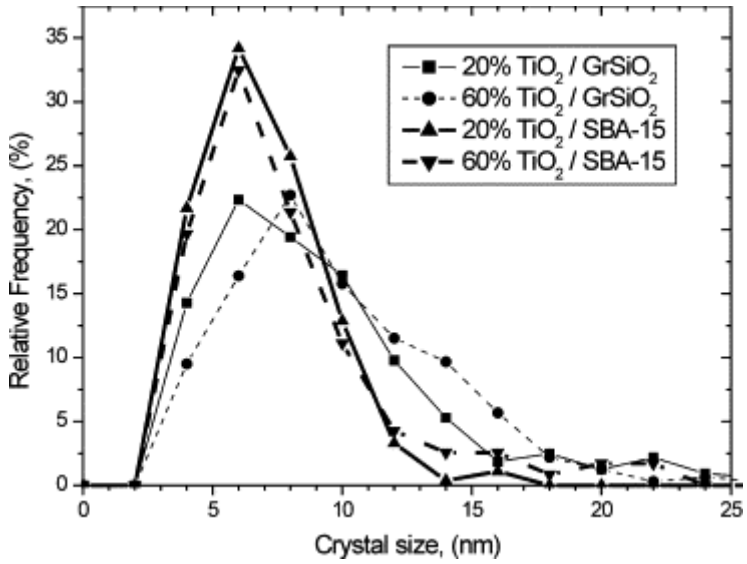

Figure 3. TiO_2 crystal size distributions of the catalysts supported on amorphous and mesostructured SBA-15 silicas.

For the catalysts with 20wt% of TiO_2 the distribution of frequencies obtained with the SBA-15 silica is narrower than that using $GrSiO_2$ as support. For higher titania content, differences induced by both supports are more pronounced. Whereas the 60%TiO_2/SBA-15 material keeps a titania crystal size distribution very similar to that of 20%TiO_2/SBA-15, the 60%TiO_2/$GrSiO_2$ catalyst shows a shift to bigger TiO_2 crystal sizes in comparison to the catalyst with 20wt% of TiO_2. These results are in agreement with the average TiO_2 crystal sizes shown in table 1.

The TEM micrograph of the 20%TiO_2/SBA-15 material shown in figure 2 also displays a clear correlation between the regular pore size of the mesostructured SBA-15

support and the crystal size of the titanium dioxide. Additionally, this micrograph also shows that the TiO_2 clusters are located inside the porous of the support with apparently no agglomeration. Consequently, it can be concluded that the SBA-15 pores produce restrictions to the TiO_2 growing, leading to size-controlled silica-supported TiO_2 photocatalysts as it was previously reported [32]. Similar phenomenon has been reported in the literature for the synthesis of particles and nanowires of PbS [35], CdS [36], silicon [37], silver [38,39], gold [39], platinum [39] and palladium [40].

One important question to answer about the TiO_2/SBA-15 catalysts is the possible existence of pore clogging of the mesoporous channels by the titanium dioxide crystals. The presence of these particles inside the pores of the SBA-15 would suggest the existence of diffusional problems, especially for high titania loadings. However, the results of pore volume reported in table 1 discard this phenomenon, at least for the low molecular size of the molecular nitrogen used for the isotherms. In fact, the pore volume of the supported photocatalysts is consistent with their silica content. In a previous work [32] we suggested that the micropore network that some authors have identified interconnecting the mesoporous channels [41,42] could be responsible of the total absence of pore clogging effects. The formation of this micropores is produced during the synthesis stage of the SBA-15 silica and is due to the penetration of the polyethylenoxide chain in the silica walls, leading to micropores when calcinating. A recent work [43] has demonstrated the correlation between the micropore structure of these materials and the treatment followed for surfactant removal. Argon adsorption isotherms in the range of very low pressures were collected, in order to obtain information about the microporous structure of the TiO_2/SBA-15 materials. The micropores size distributions have been calculated by applying the *Hovart-Kawazoe* method. For the SBA-15 a very narrow distribution with a maximum in 1.05 nm is obtained. Regarding to the 20%TiO_2/SBA-15 photocatalyst, a wider plot is found with a maximum in 1.30 nm. This broadening is probably due to both the hydrothermal treatment followed for the titanium dioxide crystallization and some microporosity generated by the titania particles located in the mesoporous channels.

Additionally, the micropore and mesopore volumes of these materials can be estimated by using the *t*-plot graphs calculated from the adsorption branch of the nitrogen adsorption-desorption isotherms. The *t*-plot graphs of the SBA-15 related materials could be divided in two zones: Zone I (at low partial pressures) is related to the micropores, and the extrapolation of the lineal part of the graph leads to the micropore volume of the material; Zone II (at

intermediate-high partial pressures) is related to the mesopores leading by extrapolation to the sum of micropores and mesopores volumes. The results obtained for the SBA-15 silica are 0.145 cm^3 g^{-1} of micropores and 0.681 cm^3 g^{-1} of mesopores. These values represent the 15.0% and 70.8% respectively of the total pore volume shown in table 1.

Concerning the 20%TiO_2/SBA-15 photocatalyst, 0.114 cm^3 g^{-1} of micropores and 0.493 cm^3 g^{-1} of mesopores are obtained, representing the 14.8% and 63.9% respectively of the total pore volume of this material. Taking into account that the nanocrystals of titanium dioxide incorporated to the silica can be considered as non-porous, all volumes calculated for the supported catalysts are consistent with the 80% of silica content. Micropore volume fraction is very similar to the support whereas the lower mesopores volume is consistent with the presence of the titanium dioxide particles inside the channels.

Results for 20%TiO_2/SBA-15 definitively establish the existence of a microporous network similar to that of the SBA-15 structure. Consequently, we propose for the TiO_2/SBA-15 photocatalysts the structure schematized in figure 4. It can be considered that these materials are constituted by TiO_2 crystals located inside the channels of the support, whose walls constrain their growing in the synthesis stage. According to this structure, diffusion could be mainly restricted to the micropore network interconnecting the mesopores.

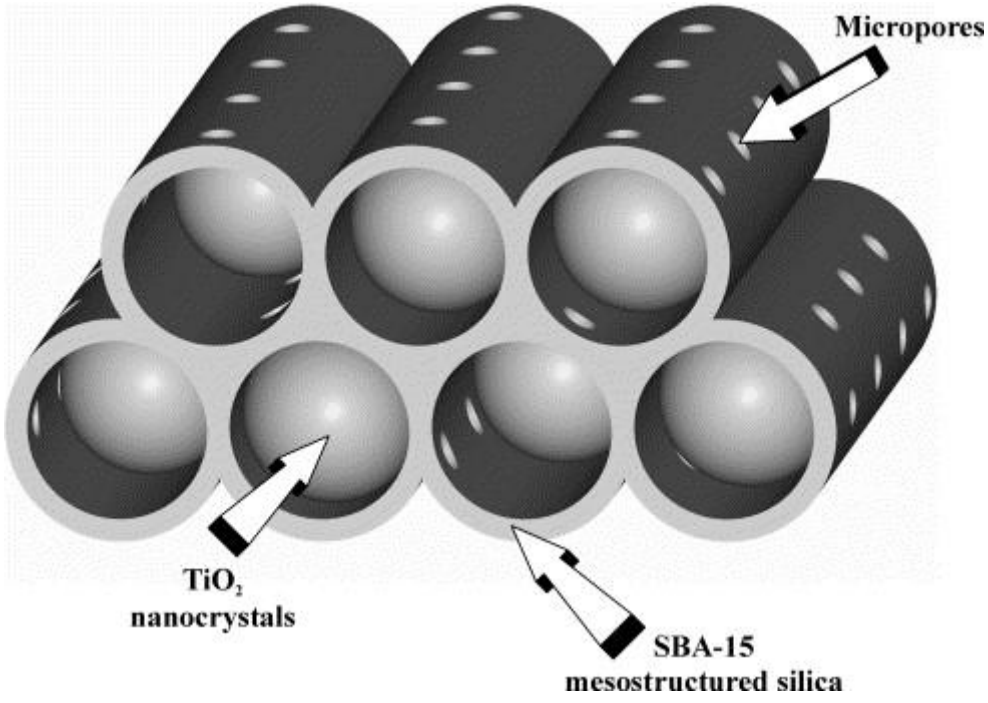

Figure 4. Schematic representation of the structure proposed for the TiO_2/SBA-15 photocatalysts.

In contrast, the results displayed in table 1 for the $TiO_2/GrSiO_2$ materials clearly show a more drastic reduction in the pore volume of these materials when increasing titania loading. Those values are even lower than that corresponding to their silica content, what means that in this case the porous structure of the support is partially clogged when incorporating titanium dioxide.

Photocatalytic activity

In order to compare the activity of the different photocatalytic materials, reaction rates must be referred to either the incident or the absorbed photon flux. These parameters, called photonic efficiency and quantum yield respectively, have been traditionally used by different authors but not always with the same meaning. In this work we use the definition and standardized protocols reported by the IUPAC [44,45]. These reports also define an additional parameter called *relative photonic efficiency* that provides a good method to compare the activity of different materials for diverse reactions and experimental conditions by using the activity of the well-known Degussa P25 TiO_2 as reference.

First of all, experiments for free cyanide photoxidation to cyanate were carried out with the supported photocatalysts. Additionally, a reaction using Degussa P25 was performed in the same experimental conditions with the aim of comparison. Table 2 reports the initial reaction rate (r^0), initial photonic efficiency (ξ^0) and relative photonic efficiency (ξ_r) for every catalyst The estimation of the maximum titania surface of every material assuming non-porous spherical semiconductor nanoparticles of TiO2 varies from 3 to 5 times the surface of the equivalent weight of Degussa P25. However the truly accessible titania surface is difficult to determine, but it must be necessary lower taking into account that these nanoparticles are supported on the silica. Consequently, although it would be more correct to compare the activity of the catalysts through the surface related reaction rate expression, we have used the volume related reaction rate expression, taking into account that this definition is widely used in the literature and from a technical point of view is more useful in order to compare the performance of the different materials for the same catalyst weight.

The photonic efficiency was calculated as the ratio between the initial reaction rate in molar units and the incident photon flow determined by potassium ferrioxalate actinometry. Concerning the values of relative photonic efficiencies, they represent the ratio between the activity of every catalyst and that obtained with P25 TiO_2 in the same experimental

conditions, either calculated as the ratio between the reaction rates or the photonic efficiencies.

Table 2. Activity of the catalysts for different cyanide species photodegradation.

Free Cyanides	$\mathbf{r^0}$ ($mg_{CN}\,l^{-1}min^{-1}$)	ξ^0 ($mol_{CN}\,Einstein^{-1}$)	ξ_r
Degussa P25	1.5400	0.0722	1.0000
20% TiO_2/$GrSiO_2$	0.7514	0.0352	0.4879
40% TiO_2/$GrSiO_2$	0.8533	0.0400	0.5541
60% TiO_2/$GrSiO_2$	0.9838	0.0461	0.6389
20% TiO_2/SBA-15	1.0300	0.0483	0.6688
40% TiO_2/SBA-15	1.1144	0.0523	0.7236
60% TiO_2/SBA-15	1.3054	0.0612	0.8477
Hexacyanoferrate-(III)	$\mathbf{r}$ ($mg_{OCN}\,l^{-1}min^{-1}$)	ξ ($mol_{OCN}\,Einstein^{-1}$)	ξ_r
Degussa P25	0.0330	$1.545\cdot10^{-3}$	1.000
20% TiO_2/$GrSiO_2$	0.0501	$2.348\cdot10^{-3}$	1.520
20% TiO_2/SBA-15	0.2622	$1.229\cdot10^{-2}$	7.956
40% TiO_2/SBA-15	0.1619	$7.589\cdot10^{-3}$	4.912
60% TiO_2/SBA-15	0.0997	$4.673\cdot10^{-3}$	3.025
Dicyanoaurate-(I)	$\mathbf{r^{max}}$ ($mg_{Au}\,l^{-1}min^{-1}$)	ξ^{max} ($mol_{Au}\,Einstein^{-1}$)	ξ_r
Degussa P25	0.3392	$3.83\cdot10^{-3}$	1.000
60% TiO_2/$GrSiO_2$	0.4563	$5.16\cdot10^{-3}$	1.345
20% TiO_2/SBA-15	0.0982	$1.11\cdot10^{-3}$	0.289

As it can be seen from table 2, all the supported catalysts show lower activities than the P25 TiO_2 for free cyanides photoxidation. However, important differences are obtained depending on the titania loading and the kind of silica support. With both supports an increase in the photonic efficiency is obtained as the titanium dioxide wt% increases, but SBA-15 based photocatalysts always show higher activities than $GrSiO_2$ based materials with the same TiO_2 loading.

These results suggest that no diffusional problems are present in the TiO_2/SBA-15 structure and, what is more important, that the intrinsic activity of the size-controlled TiO_2 crystals of these materials are much higher than those obtained with the use of an amorphous support with an opener porous structure. This high activity, however, is always lower than the photonic efficiency achieved with the P25 catalyst, reaching at most an 85% of the latter

value with the 60%TiO_2/SBA-15 material. This fact confirms that a decrease in activity must be probably assumed when supporting TiO_2.

Further experiments with different cyanide-containing compounds were carried out in order to study de influence of the structural properties of the 20wt% silica-supported materials. Hexacyanoferrate-(III) is a metal-cyanide complex that release free cyanide to the medium on exposure to UV light. Consequently, the oxidation of cyanide to cyanate requires of a previous photolytic breakage of this complex. More details about the degradation mechanism of these complexes can be found elsewhere [46].

The reaction profiles obtained in this case show that after 2 hours of irradiation a constant production rate of cyanate is obtained. For that reason, the comparison shown in table 2 was done in these conditions because some catalysts show a clear decay in the activity with time, as it is the case, for instance, of the P25 TiO_2. Despite the high activity shown by this material for free cyanides photoxidation, a very low activity of oxidation was obtained when iron-cyanide complexes are present in the medium. In contrast, the supported photocatalysts leads to better results for the cyanide photoxidation rate, up to 8 times higher for the catalyst 20%TiO_2/SBA-15.

To study the effect of the titania loading, further experiments were conducted with SBA-15 catalysts containing 40wt% and 60wt% of TiO_2, whose results are also shown in table 2. Surprisingly, in this case a lower photonic efficiency is obtained as the titanium dioxide content increases. In order to explain this fact we must refer to the structure of these materials. If we assume that the increase in the TiO_2 loading reduces the average distance that the chemicals must diffuse inside the porous structure of the SBA-15, these results seem to indicate that the existence of mass transport problems in the low loaded SBA-15 materials could be responsible of its high activity. This hypothesis is also in agreement with the results obtained for Degussa P25 and 20%TiO_2/$GrSiO_2$. As the presence of iron-cyanide species in the medium seems to reduce the oxidation rate of the released free cyanides, the activity increases in those catalysts in which the access of the bigger iron-cyanide complexes are more restricted. Consequently, the activity increases from P25 to 20%TiO_2/$GrSiO_2$ and then to 60wt%, 40wt% and finally 20%TiO_2/SBA-15.

In order to obtain further experimental verifications for this hypothesis, experiments of photocatalytic treatment of dicyanoaurate complex solutions were carried out. The main difference of this metal-cyanide complex respect to hexacyanoferrate is that these species are stable under UV irradiation and does not produce photolytic release of free cyanide. Therefore the complex must diffuse to the TiO_2 surface and the gold atoms must be reduced to Au(0)

producing the release of free cyanides.

According to the assumption of diffusional restrictions, in this case the activity of the 20%TiO_2/SBA-15 material would be much lower than that obtained with the catalyst 60%TiO_2/$GrSiO_2$ in which the lower diffusional problems of all the supported catalysts must be found. The results of these experiments are also shown in table 2 in terms of the maximum reaction rate, achieved not exactly at the beginning of the irradiation but after several minutes. As it can be seen the photonic efficiency of the 20%TiO_2/SBA-15 catalysts is fivefold lower than that corresponding to the 60%TiO_2/$GrSiO_2$. In fact, in this case the activity of the latter is even higher than the value for Degussa P25. This effect could be due to the adsorption properties of the silica and its nature is under further investigations.

Nonetheless, these results confirm the mass transfer control hypothesis for the rate limiting step of the reaction of metal-cyanide complexes with TiO_2/SBA-15 catalysts. Since diffusional problems are not expected for free cyanides photoxidation, taking into account the lower molecular size of this ion with respect to the bigger metal complexes, this could mean that cyanide is below a critical size for diffusional control. Consequently we can conclude that TiO_2/SBA-15 photocatalysts show molecular sieve behaviour induce by the micropore network that interconnect the channels of the SBA-15 mesoporous structure.

Summarising, the activities of the different photocatalysts show the following decreasing order:

i) Free cyanides photoxidation: Degussa P25 > TiO_2/SBA-15 > TiO_2/$GrSiO_2$. In this case, the reaction is very fast, what produces that the supported photocatalysts work under diffusional control. The molecular size of the free cyanide ions is small enough to diffuse inside the porous structure of the TiO_2/SBA-15 materials leading to better results that the amorphous support, probably due to a higher intrinsic activity of TiO_2 particles grown in a restricted environment..

ii) Hexacyanoferrate photooxidation: TiO_2/SBA-15 > TiO_2/$GrSiO_2$ > Degussa P25. When iron cyanocomplexes are present in the medium, the deactivation of the titanium dioxide produces higher reaction rates when working under diffusional control, specially for TiO_2/SBA-15 materials into which the iron complexes cancan not diffuse.

iii) Dicyanoaurate photoreduction: TiO_2/$GrSiO_2$ > Degussa P25 > TiO_2/SBA-15. In contrast, the photodegradation of dicyanoaurate is so slow that also the TiO_2/$GrSiO_2$ materials work under kinetic control. In these conditions, the activity of these materials is even higher than that of Degussa P25 TiO_2, what could be due either to a higher intrinsic activity of their smaller titania crystals or to changes induced in the adsorption of the gold cyanocomplexes by

the silica. In contrast, the TiO_2/SBA-15 catalysts remain under diffusional control due to the big size of the complex.

CONCLUSIONS

The results presented in this work point out the strong influence of the textural properties of the silica on the catalytic activities of the supported TiO_2 photocatalysts. The elucidation of the structure of the TiO_2/SBA-15 photocatalysts has permitted to explain the differences observed in the photonic efficiencies shown by these materials in comparison with the use of an amorphous silica support.

As a general conclusion, it must be point out that to achieve an absolute assessment of the activity of the new developed photocatalysts several model compounds should be used. This is due to the fact that, despite the photocatalytic reaction is non-selective by itself, the mass transport limitations of the specific pollutant could control the global kinetics, specially when using supported photocatalyst in which internal diffusion is also present. Nevertheless further work must be accomplish in order to determine quantitatively the diffusion coefficients of the different chemical compounds in the supported photocatalysts.

ACKNOWLEDGEMENTS

The authors thank “Consejería de Educación, Comunidad de Madrid” for the financial support of this research through the project “Contrato-Programa Grupos Estratégicos de Investigación” and “Ministerio de Ciencia y Tecnología” through the project PPQ2000-1287.

REFERENCES

[1] D.F. Ollis, E. Pellizzetti, and N. Serpone, Environ. Sci. Tech., 25 (1991) 1522.

[2] M.A. Fox and M. Dulay, Chem. Rev., 93 (1993) 341.

[3] O. Legrini, E. Oliveros, and A.M. Braun, Chem. Rev., 93 (1993) 671.

[4] D.F. Ollis and Al-ekabi (Eds.), Photocatalytic purification and treatment of water and air”, Elsevier, Amsterdam, 1993.

[5] M.R. Hoffmann, S.T. Martin, W. Choi and D.W. Bahnemann, Chem. Rev., 95 (1995) 69.

[6] J.M. Herrmann, Catal. Today, 53 (1999) 115.

[7] D. Blake, Bibliography of work on the photocatalytic removal of hazardous compounds from water and air, NREL, Golden, CO, (May 1994; 1st update: October 1994; 2nd update: October 1996; 3rd update: January 1999; 4th update: October 2001).

[8] R.L. Pozzo, M.A. Baltanás and A.E. Cassano, Catal. Today, 39 (1997) 219.

[9] J.A. Byrne, B.R. Eggins, N.M.D. Brown, B. McKinney and M. Rouse, Appl. Catal. B: Environ, 17 (1998) 25.

[10] J.M. Herrmann and J.L. Mansot, J. Catal., 121 (1990) 340.

[11] L.J. Alemany, M.A. Bañares, E. Pardo, F. Martin, M. Galan-Fereres and J.M. Blasco, Appl. Catal. B: Environ., 13 (1997) 289.

[12] H. Yamashita, Y. Ichihashi, M. Harada, G. Stewart, M.A. Fox and M. Anpo, J. Catal., 158 (1996) 97.

[13] J.M. Herrmann, H. Tahiri, C. Guillard and P. Pichat, Catal. Today, 54 (1999) 131.

[14] V. Romeas, P. Pichat, C. Guillard, T. Chopin and C. Lehaut, Ind. Eng. Chem. Res., 38 (1999) 3878.

[15] H. Yamashita, M. Honda, M. Harada, Y. Ichihashi, M. Anpo, T. Hirao, N. Itoh and N. Iwamoto, J. Phys. Chem. B, 102 (1998) 10707.

[16] G. Lassaleta, A. Fernandez, J.P. Espinos and A.R. Gonzalez-Elipe, J. Phys. Chem., 99 (1995) 1848.

[17] H. Inoue, T. Matsuyama, B.J. Liu, T. Sakata, H. Mori and H. Yoneyama, Chem. Lett., (1994) 653.

[18] A. Yasumori, K. Yamazaki, S. Shibata and M. Yamane, J. Ceram. Soc., 102 (1994) 702.

[19] R. Castillo, B. Koch, P. Ruiz and B. Delmon, J. Catal., 161 (1996) 524.

[20] M.L. Franco-García, M. Murat, J.P. Percherancier and B. Pouyet, Fresenius Environ. Bull., 5 (1996) 563.

[21] G.P. Lepore, L. Persaud and C.H. Langford, J. Photochem. Photobiol. A: Chem., 98 (1996) 103.

[22] Q. Dai, N. He, K. Weng, B. Lin, Z. Lu and C. Yuan, J. Inclusion Phenom. Macroc. Chem., 35 (1999) 11.

[23] K. Kobayakawa, C. Sato, Y. Sato and A. Fujishima, J. Photochem. Photobiol. A: Chem., 118 (1998) 65.

[24] Z. Ding, X. Hu, G.Q. Lu, P.L. Yue and P.F. Greenfield, Langmuir, 16 (2000) 6216.

[25] Z. Ding, X. Hu, P.L. Yue, G.Q. Lu and P.F. Greenfield, Catal. Today, 68 (2001) 173.

[26] R.J. Davis, Chem. Mater., 4 (1992) 1410.

[27] Y. Xu, C.H. Langford, J. Phys. Chem. B, 101 (1997) 3115.

[28] H. Yamashita, Y. Fujii, Y. Ichihashi, S.G. Zhang, K. Ikeue, D.R. Park, K. Koyano, T. Tatsumi and M. Anpo, Catal. Today, 45 (1998) 221.

[29] B.J. Aronson, C.F. Blanford and A. Stein, Chem. Mater., 9 (1997) 2842.

[30] N. Takeda, T. Torimoto, S. Sampath, S. Kuwabata and H. Yoneyama, J. Phys. Chem., 99 (1995) 9986.

[31] H. Yoneyama and T. Torimoto, Catal. Today, 58 (2000) 133.

[32] R. van Grieken, J. Aguado, M.J. López-Muñoz and J. Marugán, J. Photochem. Photobiol. A, 148 (2002) 315.

[33] J. Aguado, R. van Grieken, M.J. López-Muñoz and J. Marugán, Catal. Today, 75 (2002) 95.

[34] D. Zhao, J. Feng, Q. Huo, N. Melosh, G.H. Fredickson, B.F. Chmelka and G.D. Stucky, Science, 279 (1998) 548.

[35] F. Gao, Q. Lu, X. Liu, Y. Yan and D. Zhao, Nano Lett., 1 (2001) 743.

[36] W. Xu, Y. Liao and D.L. Akins, J. Phys. Chem. B, 106 (2002) 11127.

[37] N.R.B. Coleman, N. O'Sullivan, K.M. Ryan, T.A. Crowley, M.A. Morris, T.R. Spalding, D.C. Steytler and J.D. Holmes, J. Am. Chem. Soc., 123 (2001) 7010.

[38] M.H. Huang, A. Choudrey and P. Yang, Chem. Commun., (2000) 1063.

[39] Y.J. Han, J.M. Kim and G.D. Stucky, Chem. Mater., 12 (2000) 2068.

[40] I. Yuranov, P. Moeckli, E. Suvorova, P. Buffat, L. Kiwi-Minsker and A. Renken, J. Molec. Catal. A: Chem., 192 (2003) 239.

[41] M. Kruk and M. Jaroniec, Chem. Mater., 12 (2000) 1961.

[42] A. Galarneau, H. Cambon, F. Di Renzo, R. Ryoo, M. Choi and F. Fajula, New. J. Chem., 27 (2003) 73.

[43] R. van Grieken, G. Calleja, G.D. Stucky, J.A. Melero, R.A. García and J. Iglesias, Langmuir, 19 (2003) 3966.

[44] N. Serpone and A. Salinaro, Pure & Appl. Chem. 71 (1999) 303.

[45] A. Salinaro, A.V. Emeline, J. Zhao, H. Hidaka, V.K. Ryabchuk and N. Serpone, Pure & Appl. Chem. 71 (1999) 321.

[46] R. van Grieken, J. Aguado, M.J. López-Muñoz and J. Marugán, Appl. Catal. B.: Environ., 55 (2004) 195.